**MATERIALE PLASTICE**
*https://revmaterialeplastice.ro*
*https://doi.org/10.37358/Mat.Plast.1964*

# Mechanical Properties of Ultra-high Molecular Weight Polyethylene (Tensylon®) from Tensile Tests

**LUMINITA-CRISTINA ALIL[1], MICHEL ARRIGONI[2], CRISTIAN BARBU[1], GUILHEM BLES[2], LORENA DELEANU[3], PAVEL MOSTOVYKH[4*], SIMONA M. SANDU[5]**

[1] Military Technical Academy, 39-49 George Cosbuc, 050141, Bucharest, Romania
[2] ENSTA Bretagne, IRDL FRE No. 3744, 29806 Brest Cedex 09, France
[3]Dunarea de Jos University of Galati, Faculty of Engineering, 800008, Galati, Romania
[4]St-Petersburg State Polytechnical University, Politekhnicheskaya Ulitsa, 29, St Petersburg, Russian Federation
[5]Scientific Center for CBRN Defence and Ecology, 225 Oltenitei, 041309, Bucharest, Romania

***Abstract:*** *Results on mechanical properties of Tensylon® composites at room temperature are presented. Single-ply and two-ply samples, obtained from the ply-precursor sheet (of two orthogonal layers) have been subjected to: load till failure in traction, at different strain rates (below $10^{-1}$ $s^{-1}$) and cycles of successive loading and unloading and 5 min stress relaxation period. The characteristic times of relaxation are evaluated and the difference in values of Young modulus before and after the relaxation stage is established. A complex cyclic/relaxation test requires a visco-elasto-plastic model of Tensylon®, and allows for quantifying it. This model predicts the material behavior in other types of tests: for instance, it predicts strain rate independence of loading to failure in the considered strain rate range. Cyclic tests fulfilled at a fixed (constant) strain rate suggest that Tensylon® is an elastoplastic material without noticeable viscosity. The proposed model, additively including nonlinear viscoelasticity and plastic flow with strengthening, shows a satisfactory agreement with experimental data. It also agrees that the material is strain-rate-insensitive in the range $10^{-3}$ $s^{-1}$–$10^{-1}$ $s^{-1}$.*

***Keywords****:criss-cross composites, quasi–static tension, stress relaxation, viscoelasticity, viscoelastoplasticity, UHMWPE, Tensylon®*

## 1. Introduction

Ultra–high molecular weight polyethylene (UHMWPE) is a highly crystalline thermoplastic polymer with a repeating unit $(C_2H_4)_{n/2}$ or $(CH_2)_n$. According to [1], n has the order of $10^5$. UHMWPE is processed from polyethylene, which is obtained, in turn, by the polymerization of the ethylene monomer, $C_2H_4$. UHMWPE oriented materials are obtained from UHMWPE powder using two major techniques. One of them is the gel-spinning route [2], that includes preparation of a suspension of UHMWPE powder in a solvent by its heating, spinning it into fibers, followed by cooling and subsequent extensive hot-drawing. Another is the melt spinning route [3], followed by a combination of solid-state extrusion (SSE) and drawing, resulting in an oriented tape. Having emerged in the late 1970s, with the subsequent commercialization under the tradenames of Dyneema® produced by DSM™ and Spectra® produced by Honeywell both by gel-spun technology, UHMWPE fibers have been extensively used in the ballistic protection field in the form of soft and hard ballistic composites.

Over the years, DSM™ numerous grades of Dyneema® have been extensively studied and presented in scientific papers and it still represents, as a trademark so popular, an inexhaustible source of research activity. However, generalizing this specific product behavior to all UHMWPE composite materials, can be misleading. With more and more emerging trademarks with unique features, dependent on the manufacturing technologies and quality of raw materials and processes, it is essential to characterize each of them separately.

Our material of interest is Tensylon®, manufactured by DuPont™, better known for commercializing the aramid fiber Kevlar®, also intensively used in the ballistic protection field.

**email: mostovykh@gmail.com*

Tensylon® is representative for the SSE technique, along with other trademarks in use, such as Endumax® (Teijin). Tensylon® UHMWPE material is marketed as an oriented tape [3]. There are very few references in the literature on Tensylon® composites. For instance, Ruiz et al. [4] have performed a few exclusive ballistic performance tests, whereas O'Masta et al. [5] considered it as a material of secondary interest, while Dyneema® was not available in the laboratory.

Tensylon® laminates exhibit some advantages over Dyneema®-based laminates. Firstly, the production route of Tensylon® is cost-effective. Secondly, it requires lower pressing load during manufacturing of hard ballistic plates (15.2 MPa/120°C with our industrial partner SC STIMPEX SA, as compared to 20.6 MPa/127°C on Dyneema® [6]). However, Tensylon® chemical characteristics, such as structure, are still not described in the open literature. As Hine at al. [3] suggest, Tensylon® uses low density polyethylene (LDPE) as a matrix, and contains unidirectional filaments of several μm in diameter. These filaments are not produced separately, and cannot be mechanically characterized separately from the composite (unlike the case of Dyneema® or other classes of fibers).

Gel-spun UHMWPE fibers are less creep–resistant than carbon or aramid (Kevlar®) fibers [7]. Viscoelastic properties in Dyneema® and Spectra® laminates have been reported in [8, 9]. To the authors' knowledge, there is no published work on viscoelasticity Tensylon® or other melt–spun high–modulus UHMWPE products.

Thus, the primary goal of the present study is to characterize the viscoelasticity of Tensylon® (HSBD 30A oriented tape) [10] at room temperature. Single-ply and two-ply samples, made of one and two plies (ply-precursor tape), respectively, have been used as samples in the experiments. The tests included simple loading to failure at different strain rates, cyclic loads and tests including stress relaxation. It was revealed that stress relaxation of Tensylon® follows the generalized Maxwell (Wiechert) model of viscoelasticity. It describes both the normal stress relaxation occurring after loading Tensylon® in tension and holding, and negative (inverse) stress relaxation that happens after partial release of tensile strain with subsequent holding. The paper includes a visco-elasto-plastic model describing the totality of experiments fulfilled with Tensylon® (except the failure processes). The material constants are evaluated, formulating a constitutive law for this material. Since the rigid plates are normally made of ply–precursor tape that consists of two plies ([$0^o$/$90^o$]), these data could be extrapolated on the final products and implemented in a FE code.

## 2.Materials and methods

### 2.1. Sample preparation and experimental set–up and testing equipment

The tests were performed on a Lloyd LR5KPlus universal materials testing machine with the The tests were performed on a Lloyd LR5KPlus universal materials testing machine with the maximum force of 5 kN. Two load cells were used, with the maximum loads of 1 kN and 5 kN, respectively. According to its datasheet [11], this tensile machine records the force applied with a load cell accuracy of <0.5%, the displacement of the upper clamp with an extension resolution of $<10^{-7}$ m, and ensures the prescribed constant crosshead speed in the range of 0.01-1016 mm/min, with accuracy of ±0.2%.

The strain was, in addition to machine displacement, directly measured using the Lloyd Laserscan 200 extensometer. The Laserscan 200 is a non-contact He-Ne laser extensometer (wavelength 632.8 nm), using a 80 Hz scanning beam to illuminate the sample and the gauge markers, facilitating the set up and alignment. This optical extensometer produces a measure signal that is proportional to the distance between two reflective markers on the path of the laser beam. These two reflective markers, stuck on the tested sample, denote the gauge length of the sample - the laser takes into account only their bottom edges, regardless of their shape. For each individual sample, a pair of markers was cut out from a gray reflective adhesive tape. Each marker had approximately 0.01 m in width and a length to fit the sample width, as illustrated in Figure 1.

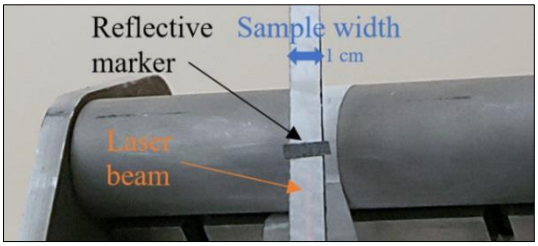


**Figure 1.** Reflective adhesive marker installed on the sample

Two types of clamping systems have been used: a pair of serrated wedges with a 0.020m x 0.040m grip surface Figure 2a) and a pair of custom–made rolls of aluminum, especially designed for tensile tests on fabric materials [12] (Figure 2b). The roll allows for a linear type grip when a rectangular planar part is pushed against it, sandwiching the sample (Figure 2c). When using the clamping systems, the laser beam had to be isolated from the metal parts using a paper sheet protection.

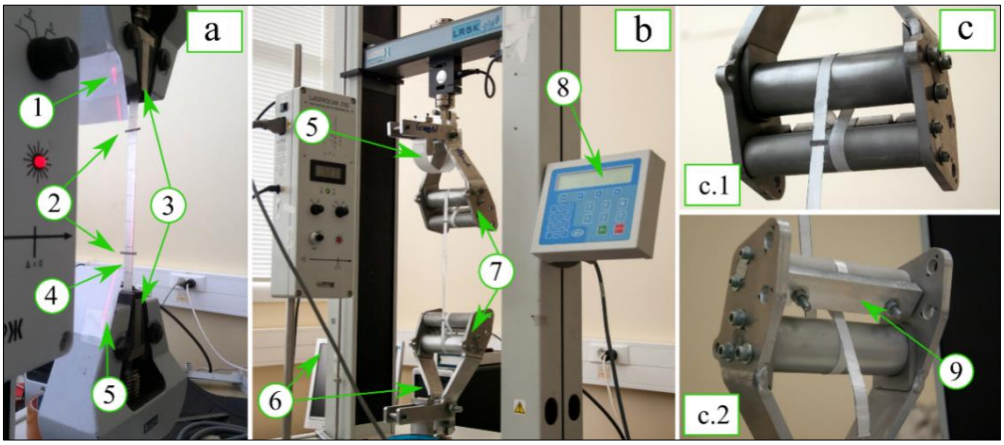


**Figure 2.** a. Serrated wedges and laser setup (pictured: active length of the sample 0.20 m); b. Clamping rolls and laser setup (pictured: active length of the sample approximately 0.30 m); c. Details of the clamping rolls (c.1 - front view and c.2 - back view); Illustrated elements: 1-laser beam; 2 - reflective markers; 3 - serrated wedges; 4 - sample; 5 - paper protection; 6 - digital control (machine + laser); 7 - clamping rolls; 8 - manual machine displacement control; 9 - rectangular piece for gripping.

## 2.2. Single-ply samples

Tensylon® HSBD 30A, the UHMWPE material used in this study, is marketed as a "High modulus bidirectional laminate for ballistic applications" [10] and is available in rolls of two orthogonal, unidirectional plies, glued together and known in the literature under the name of "pre-preg" [13] or "ply-precursor" material [14].

Single-ply samples were obtained by detaching one layer from the other in the ply–precursor tape, obtaining two different types of samples (types A and B, in our tests), characterized by the fibers' original orientation. Thus, samples A denote the length–oriented fibers in the ply–precursor tape, and samples B denote the width–oriented fibers. For each type, samples of two sizes were prepared. They had the same width of (10±0.5) * $10^{-3}$ m, and differed in their active length (length between the clamps): (50±0.5) * $10^{-3}$ m and (200±0.5) * $10^{-3}$ m. For gripping, (40±0.5) * $10^{-3}$ m of length was additionally left on both ends. They were tested using the serrated wedges clamping system. It turned out that the clamping is not sufficient enough: with low gripping force, the sample could slip, whereas with high gripping force, the sample has always been ruptured at the edge of the clamp, being damaged by the sharp gripping corner. In order to avoid these issues, a coat of Scotch® adhesive tape was added around the gripping area. It ensured that the sample broke away from the clamps.

### 2.3. Two-ply samples

Two–ply samples are denoted type D in our tests. They represent cut–outs from the ply-precursor tape, which contains two plies of unidirectional filaments. They were tested using the clamping rolls and the laser extensometer, placed at about 0.30 m away from the sample. For samples D, the active length was considered to be between the two rolls, starting perpendicularly (Figure 3). This distance was measured before each test, and used in approximate strain calculation, based on the machine displacement data. It turned out that for the tested long samples, the change in the sample active length due to its sliding on the rolls did not exceed 15% of the sample total elongation. Before each test, each sample has been weighed with $10^{-7}$ kg precision on a Precisa balance. Since the sample thickness, being of the order of $10^{-4}$ m, varies at least 10% of its value from point to point, we did not rely on these direct measurements to evaluate the stress in our samples. Instead, we used an average thickness determined based of the sample weight (mass), with a density of 940 kg/m$^3$ in compacted state and the other two linear dimensions measurements (for which we estimate a $10^{-4}$ m accuracy). The average thickness obtained in this way was used for engineering stress calculation.

### 2.4. Testing procedure

Before each test, the load cell was set to zero. Therefore, the weight of the upper wedge clamp was not included in the force; on the contrary, the weight of the lower wedge clamp was included in the force as long as the lower clamp lifted from its placement (due to the force exceeding its own weight of 8.5 kg). Each sample has been mounted on the appropriate clamping system, such as to be slightly in tension (<20 N) before the start of the test loading.

As the obtained results show, it was still an insufficient precaution, and the sample absolute strain values were not possible to calculate. However, the relative strain variation at high stresses (above 100–150 MPa), the associated Young modulus and the energy at break could be calculated with reasonable accuracy.

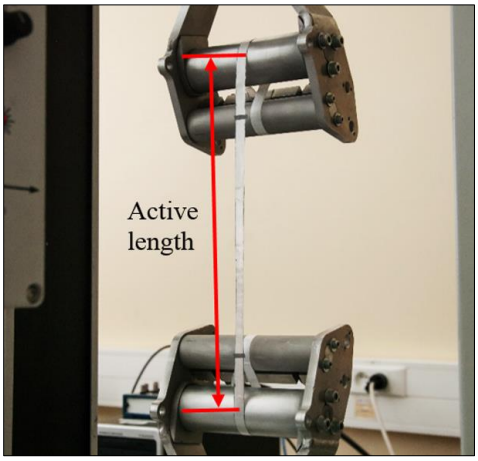


**Figure 3.** Active length of the samples when mounted on the rolls (pictured: active length approximately 0.30m)

Relaxation is defined by keeping the sample at a given strain value for a prescribed time duration. This time duration has been set to a minimum of 5 min, in accordance with reference [12], in order to assess the time dependency of the material. A number of limited tests involving relaxation of the sample have been performed, therefore the description of these specific experiments will be included in results section.

## 3. Results and discussions

### 3.1. Simple loading until failure at different strain rates

The measured displacement–time curves on Lloyd LR5KPlus machine, under constant strain rate testing, experienced noise of up to $\pm 4*10^{-5}$ m of displacement. This source of inaccuracy is, however, lower than the inaccuracy associated with clamping and machine rigidity, that will be assessed in the following by comparison to the extensometer data. We used sufficiently long samples and recalculated

the machine displacement measurements for the sample strain, solely dividing by its length, i.e., neglecting deformations of the clamping system.

### 3.2. Simple loading until failure at different strain rates

Several tests involving various strain rates, ranging from $8*10^{-5}$ $s^{-1}$ to $8*10^{-2}$ $s^{-1}$ have been performed. A typical post-mortem view of a single-ply sample is presented in Figure 4. Due to the material inhomogeneity in the longitudinal direction, its tensioning along the filaments is accompanied by some minor shear stresses (that balance unequal local strains in the width direction). As a result of the sample negligible strength in the lateral direction (since there are no filaments along the width of the sample, strength in the width direction represents the strength of pure matrix), the sample first failed in shear to become a set of thin bunches of unidirectional filaments. At slightly higher applied force, these bunches broken independently of each other and the positions of failure sections varied from one bunch to the other.

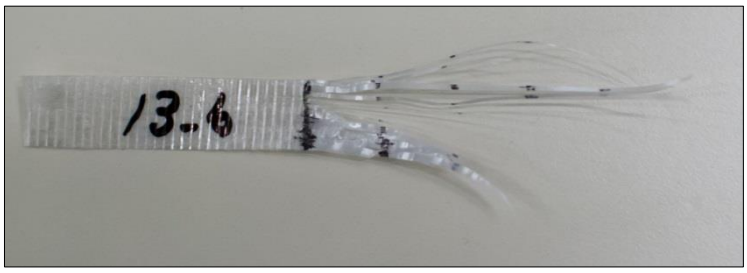


**Figure 4.** Post–mortem view of a single-ply sample
(pictured: a type B sample – width-oriented fibers)

A slight difference in modulus values was observed between samples A and B, which might be due to A slight difference in modulus values was observed between samples A and B, which might be due to the difference in the percentage of matrix contained by each separated ply. Actually, since samples A with 0.200 m active length have an average mass of $(135\pm7)\times10^{-6}$ kg, while samples B have $(165\pm7)\times10^{-6}$ kg with the same dimensions, the mean thickness also differed with 20%: $(51\pm3)\times10^{-6}$ m for type A samples and $(63\pm3)\times10^{-6}$ m for type B samples. Remarkably, failure occurred differently in the two types of samples: whereas most type A samples broke "in steps", type B samples were more likely to break throughout their width, simultaneously.

Figure 5 shows the stress–strain curves of several A and B samples, at two different strain rates: $8.3\times10^{-4}$ $s^{-1}$ (10 mm/min, with 0.200 m length) and $8.3\times10^{-3}$ $s^{-1}$ (100 mm/min with 0.200 m length). The figure also illustrates the difference between scaled machine displacement (measured by Nexygene) and the sample strain (measured by the laser extensometer). The stress–strain curves are shifted (along the strain axis) in order to superimpose, to facilitate comparison, but the zero strain has not been established (the primary reason is that single–ply samples do not keep their shape under bending even under their own weight; therefore, until the bottom clamp rose from its free placement during the loading, some sample displacement both along the acting force and perpendicular to it was inevitable in the used set–up). Since the sample failure occurs in a ductile manner, we assume that the material can be characterized with a failure strength in terms of stress but, of course, a strain to failure (also named strain at break) could be established.

The corresponding Young moduli are 92.17±0.2 GPa (A-15), 86.55±0.15 GPa (A-16), 56.12±0.1 GPa (B-4) and 56.90±0.05 GPa (B-8) at the test rate of 10 mm/min, respectively 64.60±0.15 GPa (B-12-Nexygen) and 57.5±0.4 GPa (B-12-laser) at 100 mm/min. Therefore, for a given strain rate and sample type the stress-strain curve is reproducible, although there is a ±10% sample-to-sample variability of the Young modulus evaluated under load.

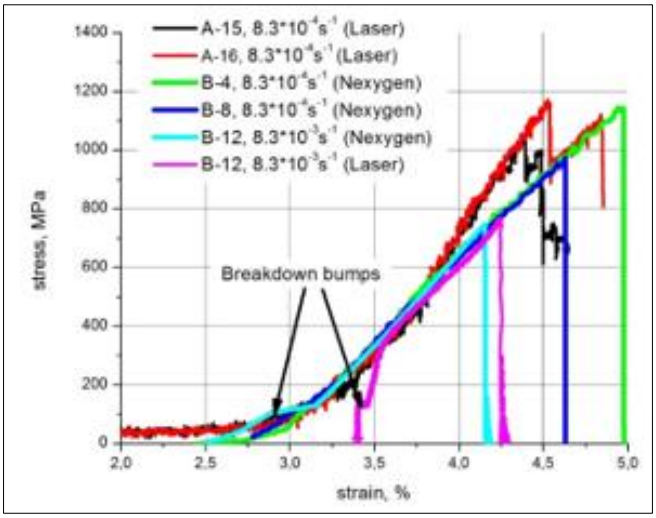


**Figure 5.** Stress–strain curves of single-ply samples in tension experiments (i.e. tension along the filaments direction) experiments at a constant strain rate until failure. Since single-ply samples have the thickness around $6*10^{-5}$m and have no stiffness in bending, the strain measurements should be interpreted as relative (it turned out impossible to exactly specify the "undeformed non-bent" length of the samples)

The curves corresponding to the higher strain rate show a peculiar breakdown bump, when the force decreases for a short amount of time. It is related to the dynamics of the bottom wedge clamp. Before the force exceeds its weight, it is lying in its mount. At a high strain rate, it gets pulled fast, gains some momentum while rising, and then causes a release wave in the sample. These effects are hard to be accounted for; therefore, Young moduli were calculated based on the stress data above 400 MPa and up to the maximum stress.

Considering the averaged values obtained under different strain rates and different sample lengths, we get a diagram presented on Figure 6. Only the parts of the curves above 250 MPa and below 90% of the rupture stress were taken into account in the linear least–square regression analysis. The significantly lower values, obtained for the short samples with 50 mm active length, signify that certain slip in the serrated wedges clamps occurred (or some other parts of the tensile machine displaced). The optical measurements on the short samples were not possible to perform. For the long samples (0.200 m), the difference between the indirect strain measurements through the machine displacement and the direct optical extensometer data still occurs, but it is less significant. No statistically significant strain rate or type of sample trend is visible.

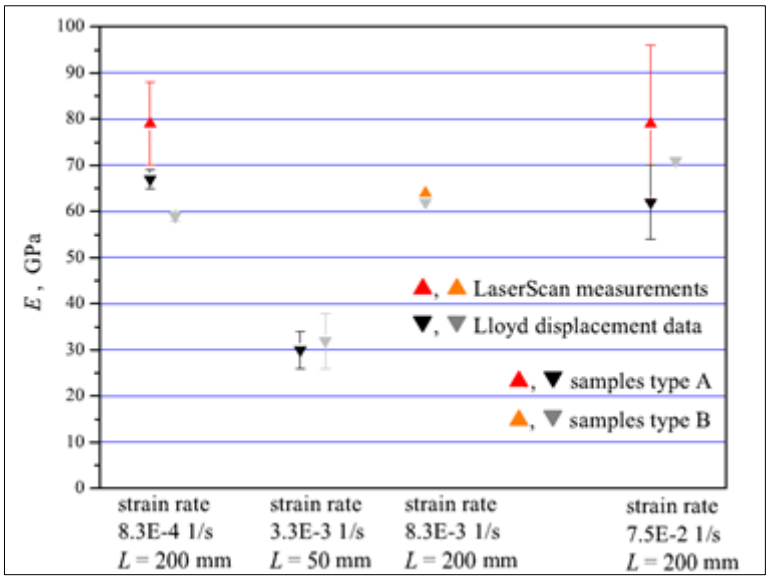


**Figure 6.** Average Young modulus in series of experiments, fulfilled under identical conditions (strain rate, length of the sample)

### 3.3. Loading-unloading successive cycles

Loading-unloading successive cycles between 100 N and 500 N (approximately between 150 MPa and 750 MPa of tensile stress) have been applied to samples B. The first two cycles were performed at 10 mm/min load-unload, and the third and the fourth cycles at 1 mm/min ($8\times10^{-5}$ $s^{-1}$). Figure 7 illustrates the sample B-15 subjected to loading-unloading successive cycles at different strain rates, and the corresponding moduli are depicted in Table 1, based on the laser measurements.

Figure 7 and Table 1 do not show any trends for Young modulus change with changing of the strain rate (we base this conclusion on the unloading phases since unloading characterizes the purely elastic behavior without any sign of plastic behavior, that is clearly evident from the lower Young moduli values on the first loadings at each strain rate).

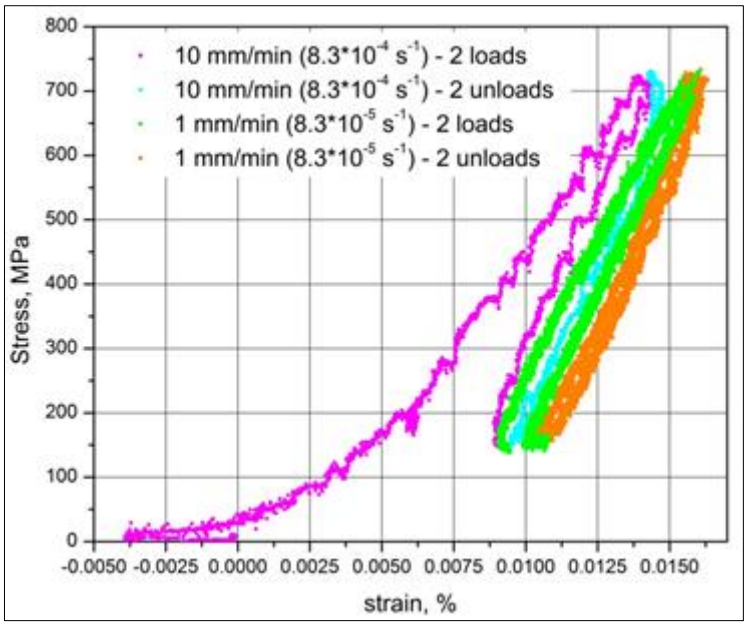


**Figure 7.** Stress-strain curves for sample B-15 at different strain rates loading–unloading successive cycles

**Table 1.** Variation of Young moduli on consecutive loading-unloading cycles in ample B-15 (color-codes of the cycles correspond to Figure 7)

| Cycle no. | Loading | | | Cycle no. | Unloading | | |
|---|---|---|---|---|---|---|---|
| | Strain rate, $s^{-1}$ | Young modulus, GPa | ± | | Strain rate, $s^{-1}$ | Young modulus, GPa | ± |
| 1-a | $8\times10^{-4}$ | 64.47 | 0.2 | 1-b | $8\times10^{-4}$ | 97.80 | 0.33 |
| 2-a | $8\times10^{-4}$ | 92.06 | 0.34 | 2-b | $8\times10^{-4}$ | 91.69 | 0.41 |
| 3-a | $8\times10^{-5}$ | 83.48 | 0.05 | 3-b | $8\times10^{-5}$ | 95.71 | 0.12 |
| 4-a | $8\times10^{-5}$ | 93.48 | 0.05 | 4-b | $8\times10^{-5}$ | 95.80 | 0.11 |

### 3.4. Relaxation cycles

Relaxation is defined by keeping the sample at a given strain value for a prescribed time duration. We performed 10 relaxation cycles on the sample B-18; each of these cycles consisted of four stages:

- loading up to 500 N (775 MPa of engineering stress using the sample weight-average thickness) at 10 mm/min ($8.3\times10^{-4}$ $s^{-1}$);
- 5 min pause at constant strain;
- unloading to 100 N (150 MPa) at 10 mm/min ($8.3\times10^{-4}$ $s^{-1}$);
- 5 min pause at constant strain.

Firstly, the real relaxation conditions were checked to coincide with the hypothetical ones (i.e., that the strain was maintained constant during relaxation). To validate this, Table 2 gives the average strain measured by the laser, during each relaxation and its standard deviation (SD).

**Table 2.** Average strain and its standard deviation ($\Delta\varepsilon$) during each relaxation, measured on sample B-18 by the laser extensometer

| Nr. | $\varepsilon$, % | $\Delta\varepsilon$, absolute % | $\varepsilon$, % | $\Delta\varepsilon$, absolute % |
|---|---|---|---|---|
| | "High" stress relaxation | | "Low" stress relaxation | |
| 1 | 1.545 | 0.007 | 1.108 | 0.007 |
| 2 | 1.753 | 0.007 | 1.227 | 0.007 |
| 3 | 1.864 | 0.007 | 1.295 | 0.007 |
| 4 | 1.937 | 0.008 | 1.361 | 0.008 |
| 5 | 2.007 | 0.008 | 1.408 | 0.008 |
| 6 | 2.056 | 0.008 | 1.466 | 0.008 |
| 7 | 2.107 | 0.008 | 1.509 | 0.008 |
| 8 | 2.140 | 0.008 | 1.559 | 0.008 |
| 9 | 2.188 | 0.007 | 1.595 | 0.008 |
| 10 | 2.215 | 0.007 | 1.632 | 0.008 |

On graphs in Figures 8 and 9, several relaxation curves in the stress–time coordinates are presented. The data of graph in Figure 8 shows normal relaxation after the sample strain was increased and stabilized, whereas graph in Figure 9 presents negative (inverse) relaxation caused by the sample strain being decreased (while still keeping the sample in tension) before stabilizing. The negative relaxation on fibrous materials was reported, for example, in [12, 13], and specifically for UHMWPE in [14]. The time t=0 for all curves correspond to the start of relaxation. These curves are commonly fitted with a Prony series representation:

$$\sigma(t) = \sum_{i=1}^{N} \sigma_{i0} \exp\left(-\frac{E_i}{\mu_i} t\right) + E_0 \varepsilon, \tag{1}$$

where the Young moduli $E_i$, i = 0, 1,…, N and viscosities $\mu_i$, i = 1, 2,…, N are either constant or slightly dependent on the strain ε at which the relaxation is fulfilled, but are independent of time. Data fitting showed that Tensylon® also follows this rule for N = 2, i.e.,

$$\sigma(t) = \sigma_{10} \exp\left(-\frac{E_1}{\mu_1} t\right) + \sigma_{20} \exp\left(-\frac{E_2}{\mu_2} t\right) + E_0 \varepsilon, \tag{2}$$

where the values $\sigma_{10}$ and $\sigma_{20}$ are determined by the previous loading history, and the relaxation times of the Maxwell elements $\tau_1 \equiv \frac{\mu_1}{E_1}$, $\tau_2 \equiv \frac{\mu_2}{E_2}$ and $E_\infty$ are material characteristics.

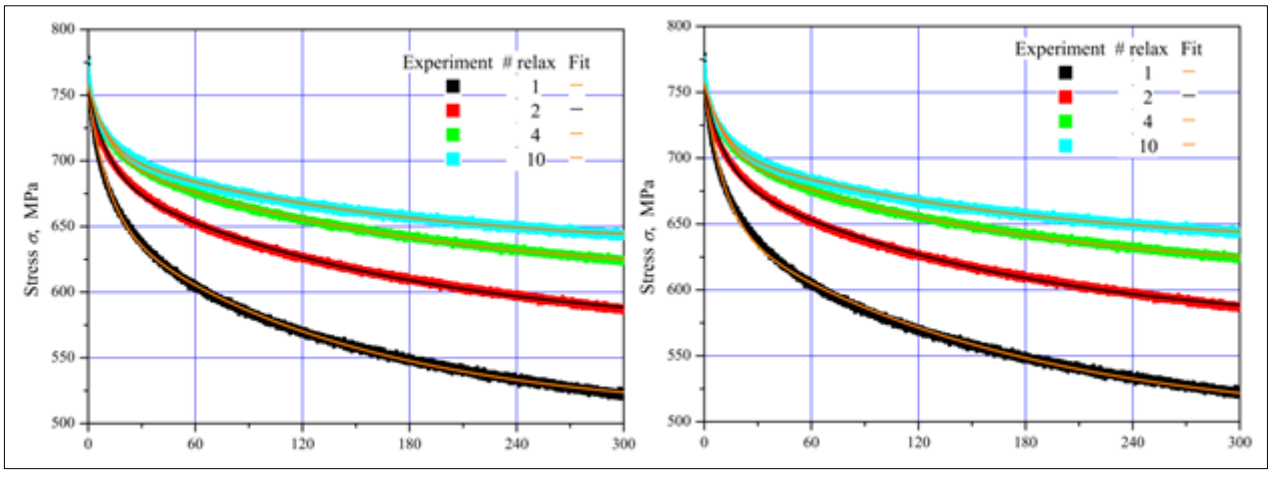


**Figure 8.** Consecutive relaxation curves done at "high" force 500 N on the same sample: black the first, red the second, green the fourth, cyan the tenth - in comparison to their two-term Prony series fits (black the second, orange the other ones). Left-least-square fits with five adjustable parameters (three initial stresses and two relaxation times); right - least-square fits with three adjustable parameters (three initial stresses only)

It is worth noting here that the proposed fit is more typical for thermosets than for thermoplastics; the explanation for that is related with a very narrow time-temperature range studied, so that a number of material characteristic times (of an order of magnitude hour and longer at room temperature) has not been resolved, and the Prony series terms associated with them take the linear elastic form $E_0\varepsilon$. All five fitting parameters together with the $\chi^2$ criterion ratio to the number of its degrees of freedom (DoF) and the correlation coefficient $R^2$ are summarized in Tables 3 and 4 and presented on Figures 8 to 11, left.

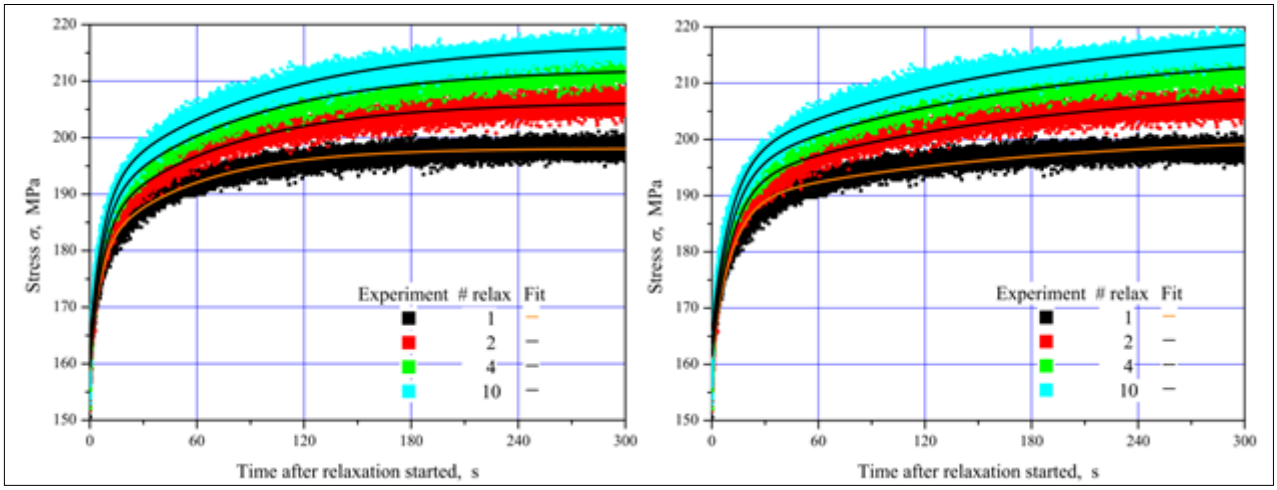


**Figure 9.** Consecutive relaxation curves done at "low" force 100 N on the same sample: black the first, red the second, green the fourth, cyan the tenth - in comparison to their two-term Prony series fits (orange the first, black the other ones). Left - least-square fits with five adjustable parameters (three initial stresses and two relaxation times); right - least–square fits with three adjustable parameters (three initial stresses only). Blow-up around the initial time (Figure 11) shows that the agreement starts at least after 2 s of relaxation

**Table 3.** Exponential decay interpolation. Data obtained on sample B-17

| No. | $\chi^2$/DoF | $R^2$ | $\sigma_{h,l}$ [MPa] | $A_1, B_1$ [MPa] | $\tau_1 \equiv \mu_1/E_1$[s] | $A_2, B_2$ [MPa] | $\tau_2 \equiv \mu_2/E_2$[s] |
|---|---|---|---|---|---|---|---|
| **1** | 1.644488 | 0.99565 | 209.99 ± 0.03 | 60.09 ± 0.03 | 220.0 ± 0.4 | 52.66 ± 0.07 | 16.89 ± 0.04 |
| **2** | 3.507767 | 0.997551 | 433.38 ± 0.06 | 122.50 ± 0.05 | 256.6 ± 0.4 | 89.72 ± 0.10 | 18.65 ± 0.04 |
| **3** | 1.01234 | 0.95801 | 175.74 ± 0.07 | 16.01 ± 0.05 | 86.3 ± 0.3 | 21.26 ± 0.08 | 6.93 ± 0.06 |
| **4** | 2.500236 | 0.997206 | 488.04 ± 0.06 | 102.68 ± 0.04 | 293.9 ± 0.5 | 62.68 ± 0.08 | 19.12 ± 0.05 |
| **5** | 0.96223 | 0.97401 | 176.85 ± 0.07 | 18.55 ± 0.04 | 116.7 ± 0.4 | 24.30 ± 0.07 | 9.84 ± 0.05 |

The fitting functions

$$\sigma(t) = \sigma_{hi} + A_{1i}e^{-t/\tau_{1i}^{h}} + A_{2i}e^{-t/\tau_{2i}^{h}} \tag{3}$$

for relaxation at "high" force and

$$\sigma(t) = \sigma_{1i} + B_{1i}\cdot\left(1-e^{-t/\tau_{1i}^{1}}\right) + B_{2i}\cdot\left(1-e^{-t/\tau_{2i}^{1}}\right) \tag{4}$$

for relaxation at "low" force were used, respectively. The fits also provided the SD of all coefficients $\Delta\sigma_{hi}$, etc. Comparing (2) to (3) and (4), we get

$$E_0\varepsilon = \begin{matrix}\sigma_{hi}(high),\\ \sigma_{1i} + B_{1i} + B_{2i}(low);\end{matrix} \tag{5}$$

$$\sigma_{10} = \begin{matrix}A_{1i}(high),\\ -B_{1i}(low);\end{matrix} \quad \ldots\ldots\ldots\ldots\ldots \quad \sigma_{20} = \begin{matrix}A_{2i}(high),\\ -B_{2i}(low).\end{matrix}$$

It can be seen that the retardation times vary only slightly from one relaxation to another, though they seem to be significantly different between "low" and "high" initial strain. To examine how significant is the retardation times variation from one relaxation to the other, an additional set of curve fitting had been performed, this time with $\tau_1$ and $\tau_2$ as fixed, and only the remaining three constants assessed during fitting. The average values $\tau_1 = 159\,\text{s}$ and $\tau_2 = 10.8\,\text{s}$, calculated at "high" initial strain conditions, were chosen as constants, and used for both "low" and "high" initial strain relaxations fitting. These fitting results are presented on Figures 8-11, right. The quality of fitting remains acceptable, so we have no reasons to think that the retardation times are stress dependent for Tensylon®. This conclusion is further confirmed by the bi-ply sample D-5 loading with relaxations presented on figure 12 (the sample of the active length between the roll clamps of 0.39 m was loaded at 10 mm/min, and kept under stress relaxation for 5 min for each of the force values 150 N, 350 N, 450 N, 500 N, 550 N, 600 N, and it broke at a force lower than 650 N - at the stress value 455 MPa, that is within the range obtained for the single-ply samples, divided by two).

Figures 10 and 11, that scale the data of Figures 8 and 9 around the initiation of stress relaxations, make it probable to assume, that the revealed two retardation times do not fully specify the material: exactly, a shorter relaxation time of an order of 1 s is likely to exist. The executed experimental procedure does not allow for experimentally evaluating the start of relaxation with sufficient accuracy, nor to verify that the change of the tensile machine regime was not associated with any oscillations, to use this portion of data for any quantitative estimates, though. It is worth pointing out that, in the Tensylon® traditional field of application for high strain rate loading, this relaxation time and the associated parameters are of great interest and the adequate testing is worth to be fulfilled.

**Table 4.** Exponential decay interpolation. Sample B-18

| No. | $\chi^2$/DoF | $R^2$ | $\sigma_{h,l}$ [MPa] | $A_1, B_1$ [MPa] | $\tau_1 \equiv \mu_1/E_1$ [s] | $A_2, B_2$ [MPa] | $\tau_2 \equiv \mu_2/E_2$[s] |
|---|---|---|---|---|---|---|---|
| **Relaxations at "high" initial force level (500 N). Fit Exponential Decay: Second Order.** | | | | | | | |
| 1 | 3.03029 | 0.998566 | 506.63 ± 0.09 | 152.27 ± 0.06 | 136.2 ± 0.3 | 93.63 ± 0.13 | 11.07 ± 0.03 |
| 2 | 1.784262 | 0.998458 | 570.05 ± 0.09 | 119.83 ± 0.05 | 160.7 ± 0.3 | 63.32 ± 0.09 | 11.31 ± 0.03 |
| 3 | 1.583241 | 0.99817 | 596.65 ± 0.09 | 104.03 ± 0.05 | 162.3 ± 0.4 | 55.96 ± 0.09 | 10.91 ± 0.04 |
| 4 | 1.43637 | 0.998009 | 609.45 ± 0.09 | 94.91 ± 0.05 | 166.8 ± 0.4 | 52.58 ± 0.08 | 11.17 ± 0.04 |
| 5 | 1.397222 | 0.997869 | 618.65 ± 0.09 | 89.71 ± 0.05 | 164.2 ± 0.4 | 51.75 ± 0.08 | 10.89 ± 0.04 |
| 6 | 1.486389 | 0.997433 | 622.14 ± 0.09 | 83.41 ± 0.05 | 162.0 ± 0.4 | 50.59 ± 0.09 | 10.65 ± 0.04 |
| 7 | 1.585621 | 0.997089 | 626.19 ± 0.09 | 79.79 ± 0.05 | 159.0 ± 0.5 | 50.74 ± 0.09 | 10.60 ± 0.04 |
| 8 | 1.715637 | 0.996701 | 628.74 ± 0.08 | 76.99 ± 0.05 | 154.6 ± 0.5 | 50.91 ± 0.09 | 10.41 ± 0.04 |
| 9 | 1.629073 | 0.996932 | 633.97 ± 0.09 | 78.55 ± 0.05 | 164.0 ± 0.5 | 50.28 ± 0.09 | 11.27 ± 0.04 |
| 10 | 1.65372 | 0.996575 | 633.84 ± 0.08 | 73.75 ± 0.05 | 154.3 ± 0.5 | 49.72 ± 0.09 | 10.49 ± 0.04 |
| **Relaxations at "low" initial force level (100 N). Fit Exponential Associate (ExpAssoc): Equation: $y = y_0 + A_1(1 - \exp(-x/t_1)) + A_2(1 - \exp(-x/t_2))$. Second Order.** | | | | | | | |
| 1 | 0.70252 | 0.97948 | 158.86 ± 0.07 | 16.90 ± 0.06 | 55.2 ± 0.2 | 21.34 ± 0.08 | 5.75 ± 0.04 |
| 2 | 0.92321 | 0.98308 | 159.38 ± 0.08 | 21.35 ± 0.05 | 75.4 ± 0.3 | 25.65 ± 0.08 | 6.89 ± 0.04 |
| 3 | 0.84655 | 0.98644 | 161.08 ± 0.07 | 23.25 ± 0.04 | 82.3 ± 0.3 | 25.66 ± 0.08 | 7.15 ± 0.04 |
| 4 | 0.92494 | 0.98637 | 161.75 ± 0.08 | 24.42 ± 0.05 | 84.7 ± 0.3 | 26.17 ± 0.08 | 7.17 ± 0.04 |
| 5 | 0.96271 | 0.98666 | 156.83 ± 0.08 | 25.11 ± 0.04 | 90.6 ± 0.4 | 26.64 ± 0.08 | 7.47 ± 0.04 |
| 6 | 1.02674 | 0.98578 | 160.22 ± 0.08 | 24.84 ± 0.04 | 92.7 ± 0.4 | 26.94 ± 0.08 | 7.70 ± 0.05 |
| 7 | 1.18128 | 0.98403 | 156.86 ± 0.08 | 25.48 ± 0.05 | 93.1 ± 0.4 | 26.37 ± 0.09 | 7.64 ± 0.05 |
| 8 | 1.16 | 0.98473 | 160.98 ± 0.08 | 26.18 ± 0.04 | 92.8 ± 0.4 | 26.91 ± 0.09 | 7.15 ± 0.05 |
| 9 | 1.03709 | 0.98665 | 160.26 ± 0.08 | 26.02 ± 0.04 | 95.2 ± 0.4 | 27.13 ± 0.08 | 7.79 ± 0.05 |
| 10 | 1.07415 | 0.98581 | 164.37 ± 0.08 | 25.82 ± 0.04 | 94.8 ± 0.4 | 26.74 ± 0.08 | 7.64 ± 0.05 |

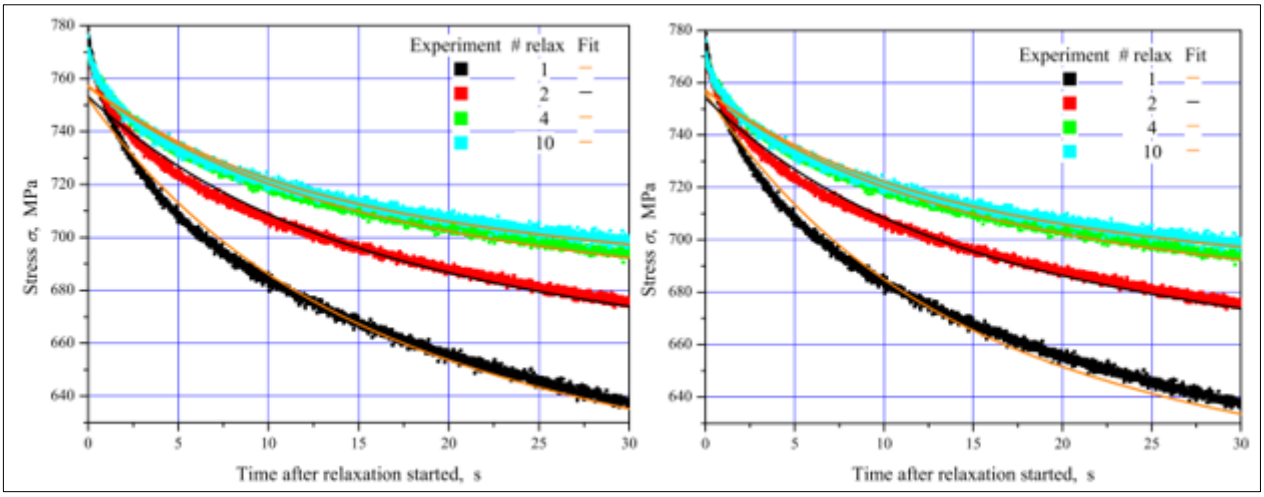


**Figure 10.** Details of Figure 8

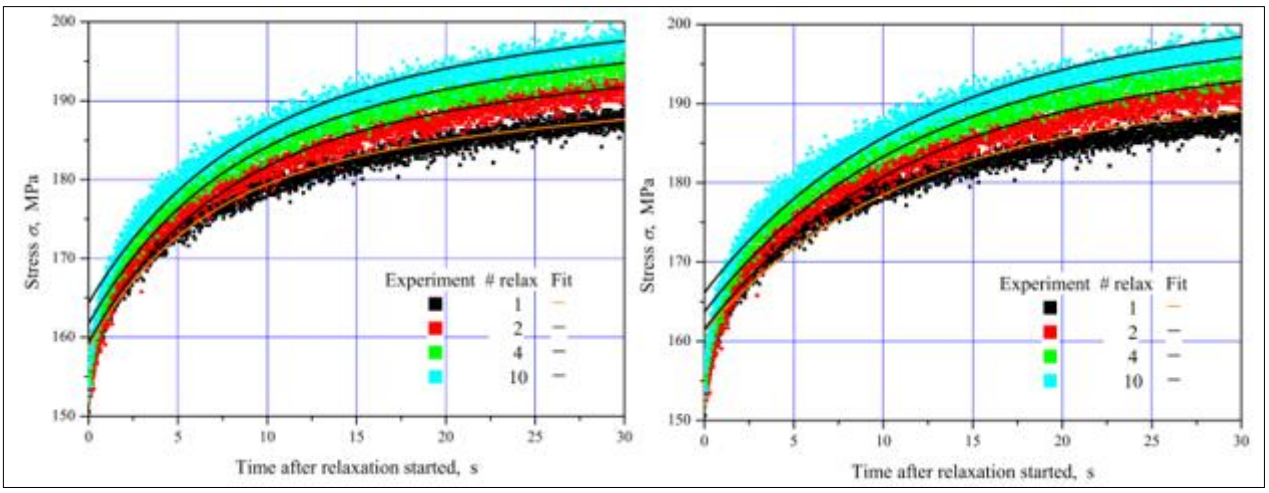


**Figure 11.** Details of Figure 9

In both Figure 10 and Figure 11, the non-exponential nature of the real Tensylon® viscoelasticity is evident, though the fitting accuracy is acceptable for prediction of material behaviour, in most similar situations.

The dependence of the fitted values $E_0\varepsilon$ as a function of $\varepsilon$ is presented on Figure 13. The magenta lines show the five-parameter fits, the black points show approximate three-parameter fits. The difference between five- and three-parameter fits is small. The group of points corresponding to the 10 relaxations, at a "high" force, forms a gradual curve, as well as the group corresponding to the 10 relaxations at a "low" force. However, no correlation between the two groups is visible. Therefore, we cannot evaluate $E_o$ from this data; moreover, we cannot propose any model describing these points (it includes spring elements with any type of nonlinearity between stress and strain).

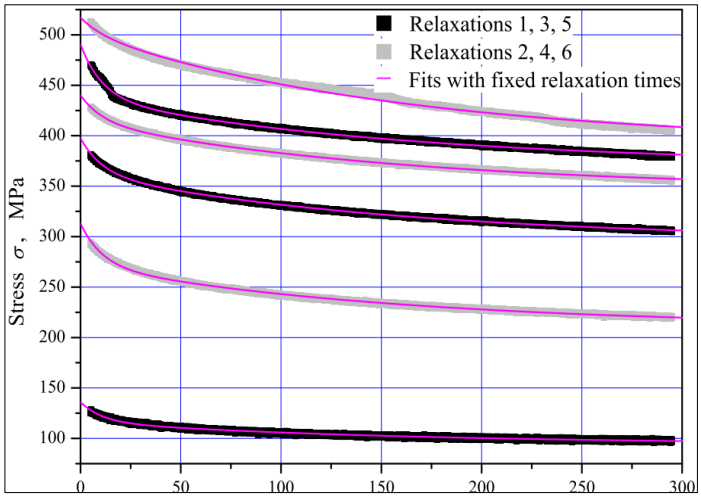


**Figure 12.** Consecutive relaxation curves obtained done with the bi-ply sample D-5. In time the curves had been shifted, whereas in stress the real values are pertained

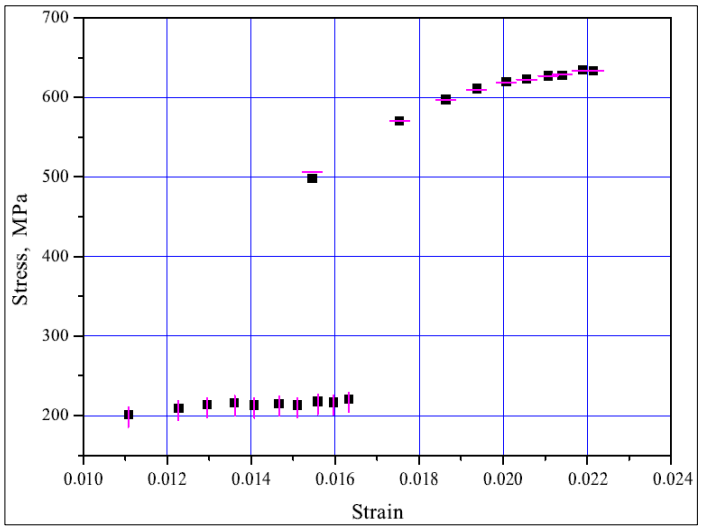


**Figure 13.** Dependence of the stress on the free spring element of the viscoelastic generalized Maxwell model

### 3.5. Evaluation of material characteristics and verification of the visco-elasto-plastic model

The results of subchapters 3.2 to 3.5 point out that Tensylon® mechanical properties are rate-independent, or at least these data do not contradict the idea of a rate-independent model for strain rates lower than $10^{-1}$ $s^{-1}$. Though the simple loading curves (subchapter 3.2) resemble to a ductile elastic behavior, the cyclic tests (subchapter 3.5) showed elasto-plastic material response without a pronounced yield limit. However, stress relaxation tests presented in subchapter 3.1.3. showed significant decrease of force (up to 30%) under constant strain conditions. Therefore, just the range of strain rate between $8\times10^{-5}$ $s^{-1}$ and $8\times10^{-3}$ $s^{-1}$ is not sufficiently large to evidence viscoelasticity of Tensylon®.

The previous section has also showed that, while relatively simple modelling can (with sufficient accuracy) describe each of the parts of the testing history (a single loading, or a single unloading, or a single relaxation), the proposed linear visco-elastic model cannot describe a multi-stage testing fulfilled, for example, on the sample B-18. This claim was already clear on Figure 13, where the points give no sign of a linear regression correlation. To give another example, let us plot the Maxwell elements parameters $E_1$, $E_2$, $\mu_1$, $\mu_2$, as they are predicted by the linear visco-elastic model, and the sequence of loading (or unloading) from the final stress of the previous relaxation to the initial stress of the foregoing relaxation, at a known stress rate (Figure 14). In this calculation, we assumed that both Maxwell elements arrive at their equilibrium states by the end of the previous relaxation, so that the Maxwell element spring stresses at the beginning of the relaxation $\sigma_{i0}$ are given by

$$\sigma_{i0} = \mu_i \frac{d\varepsilon}{dt}\left[1-\exp\left(-\frac{\Delta\varepsilon}{\tau_i}\left(\frac{d\varepsilon}{dt}\right)^{-1}\right)\right],\ i=1,2. \qquad (6)$$

Here $\Delta\varepsilon$ is the strain variation during the loading (unloading) phase of the cycle, and $\Delta\varepsilon\left(\frac{d\varepsilon}{dt}\right)^{-1}$ is the loading (unloading) phase duration. This formula was derived in [16].

Table 4 provides the values of $\sigma_{i0}$ and $\tau_i$ for each Maxwell element and each cycle; the relaxation (5) can be solved with respect to $\mu_i$, and afterwards $E_i$ obtained as $\mu_i / \tau_i$. The data of Figure 14 shows that, while the "low" initial force relaxations correspond to the same values, the "high" initial force relaxations show some variation of the parameter values. More significant is the drastic difference between the two sets of points - in this sense, the results of Figure 13 are fully confirmed.

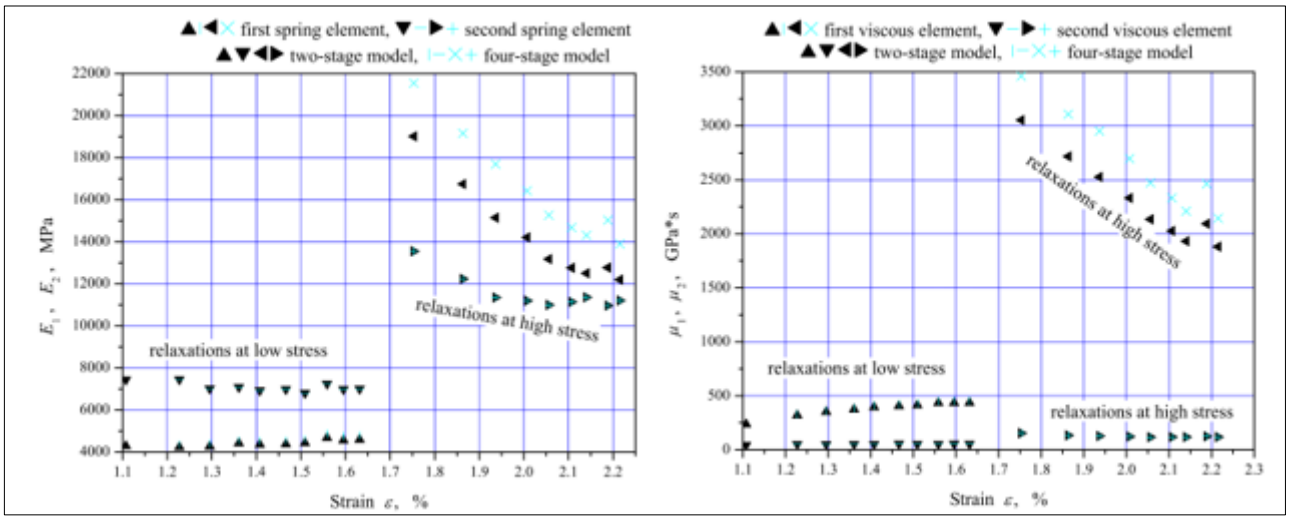


**Figure 14.** The characteristics of the Maxwell elements as recalculated from the values given using the expressions for two-stage model, $\sigma(t) = \sigma_{hi} + A_{1i}e^{-t/\tau_{1i}^{h}} + A_{2i}e^{-t/\tau_{2i}^{h}}$, and four-stage model,

$$\sigma(t) = \sigma_{1i} + B_{1i}\cdot\left(1-e^{-t/\tau_{1i}^{1}}\right) + B_{2i}\cdot\left(1-e^{-t/\tau_{2i}^{1}}\right)$$

Table 4 provides the values of $\sigma_{i0}$ and $\tau_i$ for each Maxwell element and each cycle; the relaxation (5) can be solved with respect to $\mu_i$, and afterwards $E_i$ obtained as $\mu_i / \tau_i$. The data of Figure 14 shows that, while the "low" initial force relaxations correspond to the same values, the "high" initial force relaxations show some variation of the parameter values. More significant is the drastic difference between the two sets of points - in this sense, the results of Figure 13 are fully confirmed.

The attempt to take the previous relaxation into account (that is called "four-stage model", meaning that four stage, two loading/unloading at a given strain rate and two relaxations are considered after the material is assumed to be in equilibrium, as compared to just one loading or unloading and one subsequent relaxation in the "two-stage model"), though changes the values for the "high" force relaxations for the first Maxwell element, does not reduce the discrepancy and, therefore, straight–forward complication (such as considering "six–stage model" etc.) is not a solution for reducing the noticed differences.

We adopted a different approach in order to evaluate the material characteristics within the limits of the proposed model, and in order to verify the obtained result. Namely, we are going to construct and compare the proposed model against the entity of the experimental data, presented on Figures 15 to 18.

As soon as all the material parameters are established, we can theoretically implement the same testing program as the one imposed on a testing machine. As a result, the measure of the model accuracy is the distance between the experimental and the theoretical stress–strain–time curves. Both visual and mathematical characterization of the "distance" between two curves in three dimensions is relatively complicated. Instead, we adopted a comparison on a series of different graphs (that can be viewed as "cross-sections" of the three-dimensional entity). These are:

- relaxation curves in the stress-relative time coordinates (where "relative time" is calculated from the start of the corresponding relaxation) (Figures 15 and 16);
- relaxation strain vs number of cycles (Figure 17);
- stress-strain curve, especially for the loading and unloading phases (Figure 18).

The parameters used in the simulation of relaxation curves in the stress-relative time coordinates (Figures 15, 16 and 19): elastic modulus $E_\infty = 70.8\,\text{GPa}$, viscoelastic constants of the two Maxwell elements in the Wiechert model: $E_1 = 86.1\sigma^{0.74}$, $\mu_1 = 1217\sigma^{1.18}$, $E_2 = 2053\sigma^{0.30}$, $\mu_2 = 2538\sigma^{0.56}$ (here $E_1$, $E_2$, $\sigma$ in MPa, $\mu_1$, $\mu_2$ in MPa·s), plasticity parameters: yield limit $\sigma_y = 544$ MPa, strain hardening slope $k = 15.5\,\text{GPa}$, plastic strain rate constant $g = 7{,}00*10^{-8}$ $\text{MPa}^{-1}\cdot\text{s}^{-1}$.

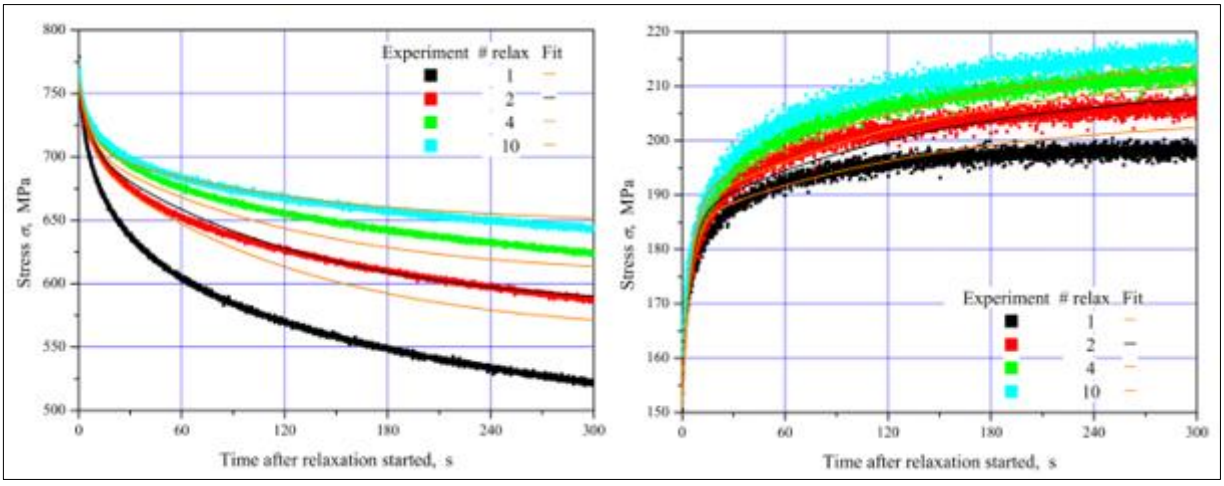


**Figure 15.** Consecutive relaxation curves done at "high" force 500 N (left) and "low" force 100 N (right) on the same sample B-18: black the first, red the second, green the fourth, cyan the tenth - in comparison to the theory predictions (black the second, orange the other ones)

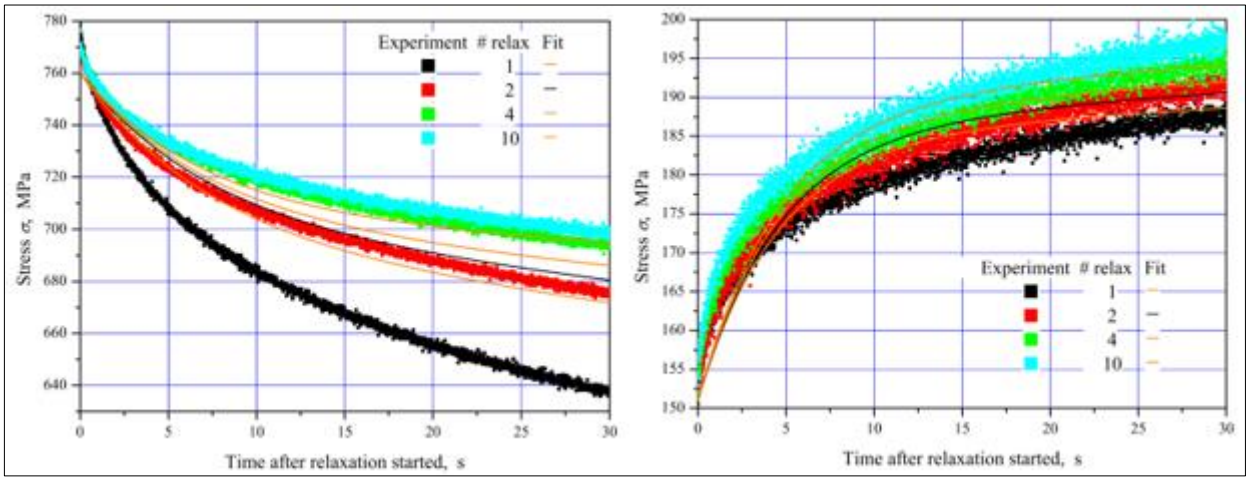


**Figure 16.** Details of Figure 15

The parameters used in the simulations of relaxation strain vs number of cycles (Figure 17) and stress–strain curve (Figure 18) are: elastic modulus $E_\infty = 70.8$ GPa; viscoelastic constants of the two Maxwell elements in the Wiechert model: $E_1 = 86.1\sigma^{0.74}$, $\mu_1 = 1217\sigma^{1.18}$, $E_2 = 2053\sigma^{0.30}$, $\mu_2 = 2538\sigma^{0.56}$ (here $E_1$, $E_2$, $\sigma$ are given in MPa and $\mu_1$, $\mu_2$ in MPa·s); plasticity parameters: yield limit $\sigma_y = 544$ MPa, strain hardening slope $k = 15.5$ GPa, plastic strain rate constant $g = 7.00 \cdot 10^{-8}$ $MPa^{-1}$ $s^{-1}$.

Figures 15 and 16 show the difference between experiment and theory predictions in stress during relaxations. Figure 17 presents the difference in strain during relaxations, and Figure 18 - the difference in both stress and strain in loading/unloading, taking into account experimental data and model evolution.

For evaluation, an indirect approach was chosen. Instead of comparing theoretical points with experimental points, the experimental data were fitted with two exponential decay (Prony) terms, and the same fits (with the same characteristic times) were implemented with respect to the theoretical relaxation curves, i.e. the theoretical data were fitted analogously to (3), (4) as $\sigma(t) = \sigma_{hi}^{th} + A_{1i}^{th} e^{-t/t_{1i}^h} + A_{2i}^{th} e^{-t/t_{2i}^h}$, $\sigma(t) = \sigma_{1i}^{th} + B_{1i}^{th}\left(1 - e^{-t/t_{1i}^1}\right) + B_{2i}^{th} \cdot \left(1 - e^{-t/t_{2i}^l}\right)$ while keeping $t_{1i}^h$, $t_{2i}^h$, $t_{1i}^l$, $t_{2i}^l$ from the fits of experimental data.

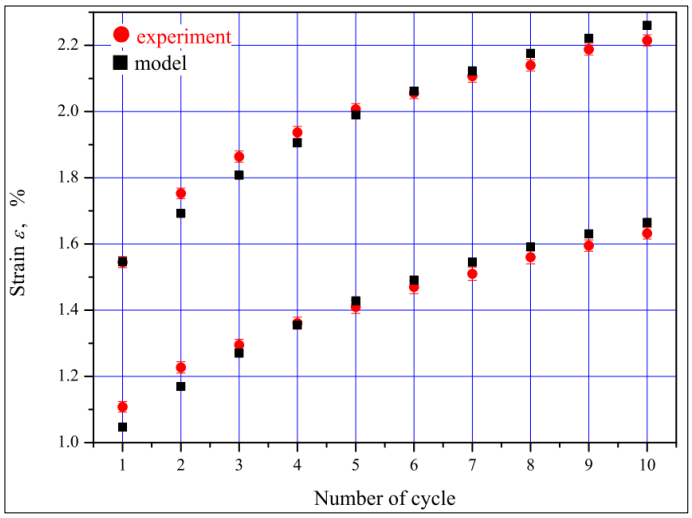


**Figure 17.** Comparison of the strains at which the sample B–18 relaxations were experimentally determined and their values from the theory predictions

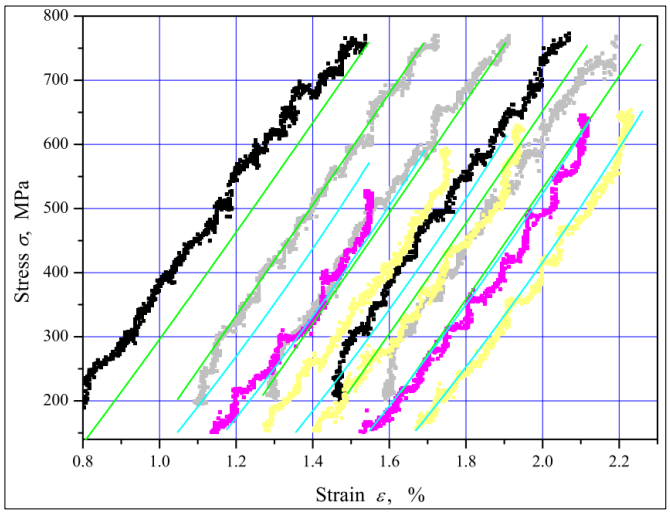


**Figure 18.** Comparison of the first, second, fourth, seventh and tenth loads and unloads. Black and light-grey points - experimental loads; magenta and light-yellow points - unloads; green lines - theoretically simulated loads; cyan lines - theoretically simulated unloads

The sum of the squared fit coefficients differences, with the addition of the squared strain at relaxation differences, was chosen as the optimization criterion. The weights in the optimization were taken as the inaccuracies of the respective experimental values (these inaccuracies have the meaning of the strain stability during holding the relaxation, rather than the measuring accuracy of the LaserScan extensometer, and the inaccuracy of the two–term Prony series fit coefficients, respectively). This criterion can be written as

$$\sum_{i=1}^{10}\left[\left(\frac{\sigma_{hi}-\sigma_{hi}^{th}}{\Delta\sigma_{hi}}\right)^2+\left(\frac{A_{1i}-A_{1i}^{th}}{\Delta A_{1i}}\right)^2+\left(\frac{A_{2i}-A_{2i}^{th}}{\Delta A_{2i}}\right)+\left(\frac{\varepsilon_{hi}-\varepsilon_{hi}^{th}}{\Delta\varepsilon_{hi}}\right)^2+\right.$$
$$\left.+\left(\frac{\sigma_{1i}-\sigma_{1i}^{th}}{\Delta\sigma_{1i}}\right)^2+\left(\frac{B_{1i}-B_{1i}^{th}}{\Delta B_{1i}}\right)^2+\left(\frac{B_{2i}-B_{2i}^{th}}{\Delta B_{2i}}\right)^2+\left(\frac{\varepsilon_{1i}-\varepsilon_{1i}^{th}}{\Delta\varepsilon_{1i}}\right)^2=minimum \quad (7)$$

The type of model to fit the data was chosen according to the following sequence of adopting more complicated ones as long as simpler models do not predict the qualitatively visible material behavior:

- linear visco-elastic modelling is incapable to describe significantly different stress relaxation amplitude at “high” and “low” stress, that is evident from comparing the experimental data on Figure 15, left and right;
- nonlinear visco-elastic modelling, that assumes the Maxwell element values $E_j, \mu_j$ as functions of the current stress applied to the material, takes this effect into account, but does not provide strain drift (i.e. the increase of the strain value at both “high” and “low” force relaxations with the number of cycles, even though the start stress value for relaxation is kept constant in all cycles) with the number of cycles, as shown on Figure 17;
- nonlinear visco-elastic accompanied with perfectly plastic modelling, that is described by the model of Sokolovsky, reviewed in [15] ($\dot{\varepsilon}_{pl}=g(\sigma-\sigma_y)$, as long as the stress $\sigma$ exceeds the yield limit $\sigma_y$), describes the strain drift, but imposes the strain gain per cycle to be constant; however, the data of Figure 17 suggests that this value decreases as the number of cycles increases;
- nonlinear visco–elastic accompanied with plasticity and strengthening modelling was assumed acceptably describing the experimental data. Strengthening was described by $\dot{\varepsilon}_{pl}=g(\sigma-\sigma_y-k\varepsilon_{pl})$, as long as the stress σ exceeds the yield limit ($\sigma_y+ k\varepsilon_{pl}$), that linearly increases with the previous plastic strain.

This last model was inspired by the linear strengthening that was revealed by the authors in [16] on the same material, but under loading in the 45° direction to the filaments. For clarity, let us note here that the strengthening equation proposed here, even though it is also linear, significantly differs from the proposed earlier in [16]: here, it relates stress, yield strain growing with plastic strain and plastic strain rate, whereas in the previous paper it related stress with plastic strain. The equation proposed earlier can be viewed as a quasi–static limit of this; in other words, the characteristic plasticity relaxation time for 45$^o$ direction tension experiments is significantly lower than that for 0$^o$ direction tension experiments. Under the same external conditions (room temperature, characteristic loading time of 10 s) 45$^o$ direction tension experiments had revealed significant plastic strain, while 0$^o$ direction tension experiments require tens of minutes for the plastic yield to occur. The plasticity with strengthening model can also be viewed as a particular case of material description [17,18]; however, we should note that the reference [17] had considered only elasto-plastic models.

The visco-elasto-plastic model used in this paper and presented on Figures 15 to 18 can be summarized in the following manner: the nominal stress and strain are decomposed into sums of the components:

$$\varepsilon=\varepsilon_{el}+\varepsilon_{pl}, \quad (8a)$$

$$\sigma = \sigma_0 + \sum_j \sigma_j; \tag{8b}$$

the spring element is described by a linear elastic model:

$$\sigma_0 = E_\infty \varepsilon_{el} \tag{8c}$$

the Maxwell elements are described by differential equations:

$$\mu_j(\sigma)\frac{d\varepsilon}{dt} = \frac{\mu_j(\sigma)}{E_j(\sigma)}\frac{d\sigma_j}{dt} + \sigma_j; \tag{8d}$$

Finally, we rewrite the plastic flow equation:

$$\frac{d\varepsilon_{pl}}{dt} = g(\sigma - \sigma_y - k\varepsilon_{pl}). \tag{8e}$$

The left-hand side of the relationship (8d) can be presented both as above and as $\mu_j(\sigma)\frac{d\varepsilon_{el}}{dt}$, i.e., either the total or only the elastic strain derivative to be included. We have not found a main reason to prefer one or the other approach. We have not evidenced any serious changes in the theory predictions, either.

Assuming the functions $E_j(\sigma)$ and $\mu_j(\sigma)$ as one-term power functions and using an iterative algorithm to minimize the criterion given by the expression (6), we obtained the 12 constants values presented in the Figures 15 to18. The values obtained from Prony series fitting and plasticity initiated around the "high" stress relaxation value were used as the starting approximation.

As a final example of the model prediction, Figure 19 compares the stress–strain curves variation with the strain rate, in the considered range (failure is not included in the model, so a fixed value of 1000 MPa is used as a cut–off). With the sample-to-sample variability present, the difference is not measurable unless very numerous series of experiments are fulfilled between 1 mm/min and the larger strain rates.

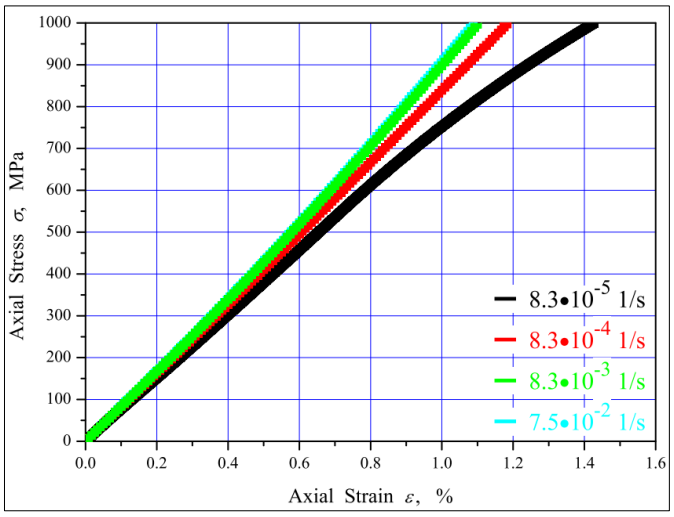


**Figure 19**. Simple loads at different strain rates, as predicted by the proposed models

The data of Figure 19 signify that the revealed characteristic times of Tensylon® relaxation are considerably larger than the characteristic time of loading in the fulfilled simple loading to failure experiments. The shorter relaxation time of the order of 1 s, that appeared not to be possible to quantify

from the fulfilled experiments, would have a stronger influence on the simple loading stress–strain curve, reflecting the strain-rate sensitivity. It can be estimated from all the fulfilled experiments that the stress variation, associated with the shorter relaxation time, does not exceed 10-20 MPa for the studied strain rates, i.e., an order of magnitude smaller than the stress variation associated with the two other experiments.

## 4. Conclusions

Strain-rate-dependent properties of Tensylon®, HSBD 30A grade, were studied. The single ply and ply-precursor tape samples have been subjected to different tensile experimental techniques (simple loading, cyclic loading, loading with stress relaxation). For the considered strain rates $10^{-3}$ -$10^{-1}s^{-1}$, it was shown that the material exhibits elastic, viscous and plastic properties, though not all of them have the same influence in each type of tests.

The simple loading tensile experiments showed a ductile linear elastic pattern under stresses above 100 MPa with significantly larger strains at low stress. Cyclic tests confirmed that the latter are permanent strains. Such stress-strain curve is typical for elastomers. Strain-rate-dependence was not pronounced among the sample-to-sample variations neither for the material elastic modulus, nor for the failure stress, at least for the tested strain rate.

To describe stress relaxation of Tensylon®, it is sufficient to use a viscoelastic model without plasticity; it is proposed in the form of the Prony series corresponding to a Wiechert schematic representation with three springs and two dashpots. It provides accurate analytical description of our 5-min relaxation experiments fulfilled at room temperature with a good correlation coefficient. The measured viscoelastic parameters turned out to be a function of the stress, i.e., nonlinearity of viscoelastic properties was revealed.

Cyclic tests fulfilled at a fixed strain rate, on the contrary, suggest that Tensylon® is an elastoplastic material, without noticeable viscosity. A combined cyclic-relaxation test (in which the sample was repeatedly loaded and unloaded, while letting the stress to relax at both stress limits) requires a joint, visco-elasto-plastic description. The proposed model, including nonlinear viscoelasticity and plastic flow with strengthening, shows the experimentally revealed behavior and a satisfactory qualitative agreement. It also agrees that the material is strain-rate-insensitive in the range $10^{-3}$-$10^{-1}s^{-1}$, but its properties it expected to change at lower strain rates around $10^{-5}$ $s^{-1}$.

Considering a wider strain rate range, either directly or through the time-temperature analogy, is supposed as the next step, in order to approach ballistic impact strain rates.

**Acknowledgments:** The authors would like to greatly thank the technical staff of ENSTA Bretagne for their invaluable help during the experimental campaign. Financial support from the ERASMUS+ program that allowed the staying of Luminița-Cristina Alil at ENSTA Bretagne is also acknowledged.

### References

1.KAVESH, S., PREVORSEK, D.C., Ultra high strength, high modulus polyethylene Spectra fibers and composites, *Int. J. Polym. Mater*, **30**, 1995, 15–56, DOI 10.1080/00914039508031459
2.van der WERFF, H., HEISSERER, U., High-performance ballistic fibers: ultra-high molecular weight polyethylene (UHMWPE), *Advanced Fibrous Composite Materials for Ballistic Protection 1 st edition, Chapter: 3,* Woodhead, 2016, pp. 71–107. DOI 10.1016/B978-1-78242-461-1.00003
3.HINE, P.J., WARD, I.M., JORDAN, N.D., OLLEY, R.H., BASSETT, D.C., A comparison of the hot–compaction behavior of oriented, high–modulus, polyethylene fibers and tapes. J. Macromol. Sci., Phys., 40(5), 2001, 959–989, DOI 10.1081/MB-100107570
4.RUIZ, R.R., GALÁN, M.A.T., CARRILLO, J.G., GAMBOA, R.A., Evaluation of ultra-high molecular weight polyethylene (UHMWPE) anisotropic configuration sample of Tensylon™, Dupont™ at medium velocity impact test. *Mex. J., Mat. Sci. Eng*., 2015, **2**, 24–32

5.O'MASTA, M.R., CRAYTON, D.H., DESHPANDE, V.S., WADLEY, H.N.G., Indentation of polyethylene laminates by a flat-bottomed cylindrical punch, *Composites Part A*, 2016, **80**, 138–147, DOI 10.1016/j.compositesa.2015.10.015
6. O'MASTA, M., DESHPANDE, V., WADLEY, H., Defect controlled transverse compressive strength of polyethylene fiber laminates, *International Journal of Solids and Structures*, 2015, **52**, 130–149, DOI 10.1016/j.ijsolstr.2014.09.023
7. DEITZEL, J., MCDANIEL, P., GILLESPIE, J., *High performance polyethylene fibers*, 2017, pp. 167–185, DOI 10.1016/B978-0-08-100550-7.00007-3
8. KROMM, F.X., LORRIOT, T., COUTAND, B., HARRY, R., QUENISSET, J.M., Tensile and creep properties of ultra high molecular weight PE fibres, *Polym. Test.*, **22**, 2003, 463–470, DOI 10.1016/S0142-9418(02)00127-7
9. LEBLANS, P.J.R., BASTIAANSEN, C.W.M., GOVAERT, L.E., Viscoelastic properties ofUHMW–PE fibers in simple elongation, *J. Polym. Sci. B Polym. Phys.*, **27**, 1989, 1009–1016, DOI 10.1002/polb.1989.090270504
10. Tensylon HSBD 30A data sheet, https://www.dupont.hk/content/dam/dupont/amer/us/en/safety/public/documents/en/DPP_Tensylon30A_datasheet_K25929_2.pdf , accessed november 2021
11. ***Ametek - Test & Calibration Instruments: LR Plus Series and EZ Series Universal Test Machine User Manual (2014). URL: http://www.ametektest.com/media/ametektest/download_links/dual_column_test_stands_lr_and_ez_manual_english.pdf
12. BLES, G., PARLIER, Y., LELOUP, R., DIB, W., RONCIN, K., JOCHUM, C., *High Tensile Stress on Fabrics of Giant Kites: "Beyond the Sea" Project*, 2012.
13. O'MASTA, M. R., Mechanisms of Dynamic Deformation and Failure in Ultra-High Molecular Weight Polyethylene Fiber-Polymer Matrix Composites, PhD Thesis, the faculty of the School of Engineering and Applied Science, University of Virginia 2014
14. RUSSELL, B. P., KARTHIKEYAN, K., DESHPANDE, V. S., & FLECK, N. A. (2013). The high strain rate response of Ultra High Molecular-weight Polyethylene: From fibre to laminate. International Journal of Impact Engineering, 60, 1-9.
15. NACHANE, R.P., HUSSAIN, G.F.S., PATEL, G.S., KRISHNA IYER, K.R., A study of inverse relaxation in some textile fibers, *J. Appl. Polym. Sci.*, **38**, 1989, 21–27, DOI 10.1002/app.1989.070380103
16. BLES, G., NOWACKI, W., TOURABI, A. Experimental Study of the Cyclic Visco-Elasto-Plastic Behavior of a Polyamide Fibre Strap, *Int. J. Solids Struct.*, **46**, 2009, 2693–2705, DOI 10.1016/j.ijsolstr.2009.02.015.
17. van der WERFF, H., PENNINGS, A.J., Tensile deformation of high strength and high modulus polyethylene fibers, Colloid. Polym. Sci., 269, 1991, 747–763.
18. VANGHELUWE, L., KIEKENS, P., Modelling relaxation behaviour of yarns part I: Extended, nonlinear maxwell model, The Journal of The Textile Institute Part I, 87, 1996, 296–304, DOI 10.1080/00405009608659082
19.BRINSON, H.F., BRINSON, L.C., *Polymer Engineering Science and Viscoelasticity: An Introduction*; Springer US, 2008, ISBN 978-0-387-73860-4
20. ALIL, L.-C., ARRIGONI, M., SANDU, S., BARBU, C., ISTRATE, M., MOSTOVYKH, P., On the Constitutive Law for the Mechanical Quasi-Static Response of Criss-Cross Composites (on the Example of UHMWPE), *Hum. Factors Mech. Eng. Def. Saf.*, **1**, 2017, DOI: 10.1007/s41314-017-0006-5.
21. MALVERN, L., The propagation of longitudinal waves of plastic deformation in a bar of material exhibiting a strain-rate effect, Journal of Applied Mechanics, 18, 1951, 203–208

Manuscript received: 22.12.2021